### Title

Bioorthogonal Chemical Imaging of Cell Metabolism Regulated by Aromatic Amino Acids.




### Authors

Bagheri, Pegah

Hoang, Khang

Kuo, Chan-Yu

et al.



### Publication Date

2023

### DOI

10.3791/65121

Peer reviewed

HHS Public Access

Author manuscript

*J Vis Exp*. Author manuscript; available in PMC 2023 December 16.

# Bioorthogonal Chemical Imaging of Cell Metabolism Regulated by Aromatic Amino Acids

**Pegah Bagheri**[*,1], **Khang Hoang**[*,1], **Chan-yu Kuo**[1], **Hetvi Trivedi**[1], **Hongje Jang**[1], **Lingyan Shi**[1]

[1]Shu Chien-Gene Lay Department of Bioengineering, University of California San Diego

## Abstract

Essential aromatic amino acids (AAAs) are building blocks for synthesizing new biomasses in cells and sustaining normal biological functions. For example, an abundant supply of AAAs is important for cancer cells to maintain their rapid growth and division. With this, there is a rising demand for a highly specific, noninvasive imaging approach with minimal sample preparation to directly visualize how cells harness AAAs for their metabolism *in situ*. Here, we develop an optical imaging platform that combines deuterium oxide ($D_2O$) probing with stimulated Raman scattering (DO-SRS) and integrates DO-SRS with two-photon excitation fluorescence (2PEF) into a single microscope to directly visualize the metabolic activities of HeLa cells under AAA regulation. Collectively, the DO-SRS platform provides high spatial resolution and specificity of newly synthesized proteins and lipids in single HeLa cell units. In addition, the 2PEF modality can detect autofluorescence signals of nicotinamide adenine dinucleotide (NADH) and Flavin in a label-free manner. The imaging system described here is compatible with both *in vitro* and *in vivo* models, which is flexible for various experiments. The general workflow of this protocol includes cell culture, culture media preparation, cell synchronization, cell fixation, and sample imaging with DO-SRS and 2PEF modalities.

## Introduction

Being essential aromatic amino acids (AAAs), phenylalanine (Phe) and tryptophan (Tryp) can be absorbed by the human body to synthesize new molecules for sustaining normal biological functions[1] . Phe is needed for the synthesis of proteins, melanin, and tyrosine, while Tryp is required for the synthesis of melatonin, serotonin, and niacin[2 , 3] . However, excess consumption of these AAAs can upregulate the mammalian target of the rapamycin (mTOR) pathway, inhibit AMP-activated protein kinase, and interfere with the mitochondrial metabolism, collectively altering macromolecule biosynthesis and leading to the production of malignant precursors, such as reactive oxygen species (ROS) in healthy cells[4 , 5 , 6] . Direct visualization of altered metabolic dynamics under excess AAA

**Corresponding Author Lingyan Shi**, Lingyanshi@ucsd.edu.
*These authors contributed equally

A complete version of this article that includes the video component is available at http://dx.doi.org/10.3791/65121.

Disclosures
The authors have no competing financial interests or other conflicts of interest.

regulation is essential to understand AAAs' roles in promoting cancer development and the growth of healthy cells[7, 8, 9].

Traditional AAA studies rely on gas chromatography (GC)[10]. Other methods, such as magnetic resonance imaging (MRI), have limited spatial resolutions, making it hard to perform cellular and sub-cellular analysis of biological samples[11]. Recently, matrix-assisted laser desorption/ionization (MALDI) has been developed to elucidate the role of AAAs in lipid and protein syntheses in cancer proliferation with noninvasive biomarkers[12, 13, 14]. However, this technique still suffers from shallow imaging depths, poor spatial resolution, and extensive sample preparation. At the cellular level, nontoxic stable isotopes, such as nitrogen-15 and carbon-13, can be traced with multi-isotope imaging and nanoscale secondary ion mass spectrometry to understand their incorporation into macromolecules. However, these methods are destructive to living biological samples[15, 16]. Atomic force microscopy (AFM) is another powerful technique that can visualize metabolic dynamics[17]. The slow rate of scanning during AFM imaging, on the other hand, may cause image distortion of the result from thermal drift.

We developed a noninvasive biorthogonal imaging modality by coupling deuterium-oxide ($D_2O$) probed stimulated Raman scattering (DO-SRS) microscopy and label-free two-photon excitation fluorescence microscopy (2PEF). This modality achieves a high spatial resolution and chemical specificity when imaging biological samples[18, 19, 20, 21, 22, 23, 24]. This protocol introduces the applications of DO-SRS and 2PEF to examine the metabolic dynamics of lipids, protein, and redox ratio changes during cancer progressions. With $D_2O$ being a stable isotope form of water, cellular biomolecules can be labeled with deuterium (D) due to its quick compensation with total body water in cells, forming carbon-deuterium (C-D) bonds through enzymatic exchange[21]. The C-D bonds in newly synthesized macromolecules, including lipids, proteins, DNA/RNA, and carbohydrates, can be detected in the cell silent region of the Raman spectrum[20, 21, 22, 25, 26, 27]. With two synchronized laser pulses, C-D bonds of newly synthesized lipids and proteins can be displayed on single cells *via* hyperspectral imaging (HSI) without extracting or labeling them with cytotoxic agents. In addition, SRS microscopy has the capability to construct three-dimensional (3D) models of selected regions of interest in biological samples by capturing and combining a set of cross-sectional images[22, 26]. With hyperspectral and 3D volumetric imaging, DO-SRS can obtain spatial distributions of newly synthesized macromolecules in single cells, along with the type of organelles that facilitate the process of promoting cancer growth under AAA regulation[22]. Furthermore, using 2PEF, we can obtain autofluorescence signals of Flavin and nicotinamide adenine dinucleotide (NADH) with high resolution, deep penetration depth, and low-level damage in biological samples[21, 23, 24]. Flavin and NADH autofluorescence signals have been used to characterize redox homeostasis and lipid peroxidation in cancer cells[22, 26]. As such, not only does the coupling of DO-SRS and 2PEF provide subcellular analysis of AAA-regulated metabolic dynamics in cancer cells with high spatial distribution, chemical specificity information, and minimal sample preparation, but the method also reduces the need to extract or label endogenous molecules with toxic reagents. In this protocol, we first present the procedures of $D_2O$ and amino acid preparation, as well as cancer cell culture. Then, we show the protocols of DO-SRS imaging and 2PEF imaging. Finally, we present the representative results of SRS and 2PEF imaging,

which demonstrate AAA-regulated metabolic changes of lipids and protein, and redox ratio changes in cancer cells. A detailed illustration of the process is highlighted in Figure 1.

## Protocol

### 1. Media preparation

1. Prepare 10 mL of control and excess AAAs in Dulbecco's modified Eagle medium (DMEM) containing 50% $D_2O$.
    1. For the control media, measure and mix 10 mg of DMEM powder with 4.7 mL of double distilled water ($ddH_2O$) in a 15 mL conical tube. The DMEM powder contains all the amino acids at standard concentrations. Thoroughly vortex and invert the tube to ensure the solution is well mixed. Add 4.7 mL of $D_2O$, 0.5 mL of fetal bovine serum (5% FBS), and 0.1 mL of penicillin/streptomycin (1%). Thoroughly vortex and invert the tube to ensure the solution is well mixed.
    2. For the 15x Phe treatment medium, measure and mix 10 mg of DMEM powder with 4.7 mL of $ddH_2O$, 0.5 mL of FBS (5%), and 0.1 mL of penicillin/streptomycin (1%) in a 15 mL conical tube. Thoroughly vortex and invert the tube to ensure the solution is well mixed. Add excess Phe powder at a concentration of 924 mg/L to the medium. Thoroughly vortex and invert the tube to ensure the solution is well mixed.
    3. For the 15x Tryp treatment medium, measure and mix 10 mg of DMEM powder with 4.7 mL of $ddH_2O$, 0.5 mL of FBS (5%), and 0.1 mL of penicillin/streptomycin (1%) in a 15 mL conical tube. Thoroughly vortex and invert the tube to ensure the solution is well mixed. Add excess Tryp powder at a concentration of 224 mg/L to the medium. Thoroughly vortex and invert the tube to ensure the solution is well mixed.
    4. Add methionine and threonine at 30.0 mg/mL and 95.0 mg/mL, respectively, to all conical tubes of the previous steps. Thoroughly vortex and invert the tube. Sodium pyruvate is not required to be added to the culture media.
    5. Filter the control and treatment media with a 25 mm syringe filter with 0.22 μm polyethersulfone membrane filters.
    6. Seal all the media-contained conical tubes with parafilm and store at 4 °C for up to 3 weeks.Prior to treating the cells with media, warm all the media to 37°C.

    NOTE: The powder and liquid reagents should be measured and combined based on the total volume of treatment and control media.

## 2. Cell sample preparation

1. Maintain cervical cancer (HeLa) cells in a culture flask (i.e., T10, T25, etc.) using standard DMEM supplemented with 10% FBS and 1% penicillin/streptomycin at 37 °C and 5% carbon dioxide ($CO_2$).
2. Sub-culture the HeLa cells at a split ratio of 1:10 until reaching 80% or higher cell viability.
3. Once the cells achieve 80% or higher confluency, proceed to seed 2 x $10^5$ cells per well onto a 24-well plate using DMEM supplemented with 0.5% FBS and 1% penicillin/streptomycin.
    1. Prior to cell seeding, prepare a 24-well plate with sterilized, poly-d-lysin, laminin-coated, round coverslips, 12 mm in diameter. Submerge the coverslips in 70% ethanol and dry gently using lint-free wipes. Place the clean coverslips in the appropriate wells of the plate.
    2. Once the cells reach 80% confluency in step 2.2, wash the cells once with 1x phosphate buffered saline (PBS) without magnesium and calcium ions.
    3. Add 0.25% trypsin to dissociate the adherent cells from the flask and incubate at 37 °C and 5% $CO_2$ for 3 min.
    4. Add DMEM supplemented with 10% FBS and 1% penicillin/streptomycin, gently pipette up and down, and collect the cells by centrifugation at 300 x *g* at room temperature (RT) for 3 min.
    5. Resuspend the cells in DMEM supplemented with 0.5% FBS and 1% penicillin/streptomycin.
    6. Count the cells using a hemocytometer, light microscope, and trypan blue, and seed a density of 2 x $10^5$ cells per well of a 24-well plate. Alternatively, an automated cell counter can be used to count the cells.
    7. Return the cells to the incubator at 37 °C and 5% $CO_2$, and gently shake the plate to distribute the cells evenly.
4. After 8 h, replace the old culture media with 50% $D_2O$/excess Phe or 50% $D_2O$/excess Tryp media. Return the cells to the incubator at 37 °C and 5% $CO_2$ for 36 h.
5. After 36 h, fix the cells on microscope slides.
    1. Prior to fixing, prepare microscope slides with imaging spacers 9 mm in diameter and place 15 μL of 1x PBS supplemented with calcium and magnesium ions.
    2. Rinse the cells with 1x PBS supplemented with calcium and magnesium ions.
    3. Add 0.5 mL of 4% methanol-free paraformaldehyde (PFA) solution and leave the plate under the biosafety hood for approximately 15 min.

4. Aspirate the PFA solution and rinse with 1x PBS supplemented with calcium and magnesium ions twice.
5. Add 1.5 mL of 1x PBS supplemented with calcium and magnesium ions in each well.
6. Use sterile tweezers to gently grab the coverslips out of each well. Invert and place the cell-containing side of the coverslips onto the imaging spacers to contact the PBS prepared in step 2.5.1. Ensure that the non cell-containing side is exposed to air.
7. Using transparent nail polish, seal the outer layer of the coverslip with the imaging spacer.

6. Store the microscope slides at 4 °C when not imaging.

## 3. Spontaneous Raman spectroscopy measurement (Figure 2)

1. Use a confocal Raman microscope to obtain spontaneous Raman spectra (Figure 2A).
2. Turn on the laser by turning the key to the **ON** position.
3. Double-click on the **LabSpec6** software icon to open the acquisition software.
4. Load the biological sample onto the sample holder directly underneath the objective lens.
5. On the software, click the **Camera icon** to turn on the video camera.
6. Adjust the focus plane to identify a region of interest with the 50x objective lens. Move the joystick to control the planer translation of the XY stage and rotate the joystick to change the depth of focus.
7. After choosing the position for measurement, switch to the 100x objective lens with 40 mW of excitation power. Click the red **Stop** icon to turn off the video camera.
8. Select a grating of 1800 lines/mm, and set the acquisition range from 400 $cm^{-1}$ to 3,150 $cm^{-1}$.
9. Set the **Acquisition Time** to 90 s, the **Accumulation** to 3, and the **Binning** to 4 for the least noise and most accurate spectrum.

   NOTE: These imaging parameters can be optimized to fit the experiment.
10. Click the **Arrow** icon to turn on the real-time display.
11. Tune the Raman shift ($cm^{-1}$) to a value of choice to fine-tune the focus plane.

    NOTE: In this experiment, the Raman laser was focused onto the lipid droplets, which contained a high concentration of $CH_2$ bonds. Therefore, a Raman shift of 2,850 $cm^{-1}$ that matched the stretching modes of the $CH_2$ bond was selected for the purpose.

12. Adjust the focus plane with the joystick to optimize the best signal-to-noise ratio.

13. After choosing the focus plane, click the red **Stop** icon for a real-time display.

14. Select the **Circle** icon to start the spectrum acquisition.

15. Once the cellular region is taken, use the same focus plane to measure the background with PBS. Subtract the background spectrum from each subcellular target spectrum using a separate computer software application, such as Origin (Figure 1B).

## 4. Imaging experiments with 2PEF and SRS

NOTE: Detailed descriptions of SRS laser alignment can be found in a prior report28 . This protocol focuses on the operation of a multimodal SRS and 2PEF imaging system (Figure 2C, D).

1. Click on **Start** to warm up the laser.

2. Follow the order to set the main switches of the control unit and the monitor on: 1) press the main switch of the control box IX3-CBH to **On**, 2) press the main switch of the touch panel controller to **On**, 3) press the main switch of the AC adapter of the power supply for LD OBIS 6 Laser Remote connected to the main laser combiner FV31-SCOMB to **On**, and 4) press the main switch of the AC adapter of the power supply for LD OBIS 6 Laser Remote connected to the sub laser combiner FV31-SCOMB to **On**.

3. Press the main switches of the Si photodiode detector and lock-in amplifier **On**.

4. Set the **Stokes Beam** at 1,031 nm, **Pulse Width** at 6 ps, and **Repetition Rate** at 80 MHz.

5. Coupled into the microscope, set the picoEmerald system supplied with the synchronized pump beam with a **Tunable Wavelength** from 720-990 nm, a **Pulse Width** of 5-6 ps, and a **Repetition Rate** of 80 MHz. The average excitation power of both the pump and Stokes is 450 mW. Optimize the excitation power to minimize photodamage for the sample.

6. Use a high-numerical aperture (NA) oil condenser (i.e., 1.4 NA) to collect the Stokes and pump beams where the sample is mounted by emitting a few drops on the condenser.

7. Mount the sample on the oil and place a large water droplet on top of the microscope slide where the sample is fixed. This is for the water-immersion objective lens.

8. Set the lock-in amplifier to 20 MHz. Process the image now using the super-resolution software module.

9. Select 512 pixels x 512 pixels and 80 μs/pixel for the dwell time.

10. Once the desired cellular region is focused properly, acquire the image. Using the acquisition software of the microscope, save the images as an Olympus .oir graphic file.

11. Acquire a background image at 1,900 $cm^{-1}$ and subtract it from all cellular images.

12. To perform 2PEF imaging, use the same tunable picosecond laser, and set the label-free autofluorescence of Flavin and NADH to 800 nm and 780 nm, respectively.

13. Use a 460 nm/515 nm filter cube to collect the Flavin and NADH autofluorescence backscattered emission.

14. Adjust the dwell time to 8 μs/pixel and the pixel size to 512 pixels x 512 pixels. Set the laser shutter power parameter to 150 mW.

15. For 3D image reconstruction, tune the stimulated Raman loss to 2,850 $cm^{-1}$ (797 nm).

16. Once the desired single cells have been identified, register the laser to scan from the top focus plane to detect the top and bottom layers of those cells.

    NOTE: 3D models are generated and saved as .oir files.

## 5. Spectra and image analysis

### 1. Spectra analysis

1. Use the Origin software or other relevant applications to subtract the background spectrum from all subcellular target spectra.

2. Use MATLAB's mathematical modeling operations to process the Raman spectra with the software's built-in functions. Python can also be used for spectra processing.

    1. Spectral pre-processing begins with converting the files into an array. The spectra are interpolated at every reciprocal centimeter.

    2. For validation, graph the raw data. Perform the baseline correction on the raw spectra using the built-in function **msbackadj** in MATLAB. In brief, the built-in function estimates baseline points at separation-unit values identified by users and returns the distance between adjacent windows. From the baseline points, estimate and draw a regression line. Apply **Smoothing** to smooth the regression line to subtract the baseline from each individual raw spectrum.

    3. Perform min-max normalization by dividing the Raman intensity of the protein at 2,930 $cm^{-1}$ by the intensity of each Raman shift. The 2,930 $cm^{-1}$ signal is typically the highest intensity on the Raman spectrum. With this normalization, the maximum value gets transformed into a 1 while the minimum value gets transformed into a 0. Every other value gets transformed into a decimal between 0 and 1.

4. Average the individual spectra of the same condition into a single spectrum to reduce noise.

3. Once processed, use applications, such as Origin, to display all the spectra simultaneously. The peaks displayed in the spectra represent a specific chemical bond or functional group.

### 2. 3D image analysis of lipid droplets

1. Use FIJI-ImageJ software to process all 3D images

2. Perform the functions **Bandpass Filters** and **Smoothing** for the 3D image stacks.

3. For 3D image analysis, assign each lipid droplet to a spherical score calculated by measuring the distance between its center of mass to the surface. Compare each spherical score with a spherical score of a perfect sphere on the same Euclidean plan. Discard lipid droplets with low spherical scores and evaluate the remaining lipid droplets for their volume and counts.

4. Analyze the volume and counts of lipid droplets between different treatments for statistical significance on an appropriate statistical software application. Here, GraphPad Prism was used.

### 3. 2D hyperspectral image analysis

1. Use FIJI-ImageJ software to process all the 2D hyperspectral images.

2. Select the 2,930 $cm^{-1}$ channel to make a mask image that contains 0 and 1 values. Assign the background to 0 and the cellular region to 1.

3. Subtract the deuterium-labeled protein channel (2,175 $cm^{-1}$) to the background channel (1,900 $cm^{-1}$) to remove the fluorescent effects.

4. Divide the resulting deuterium-labeled protein channel by the protein channel (2,930 $cm^{-1}$) to obtain protein turnover rate ratiometric images.

5. Then, multiply the mask image made in step 5.3.2 by the ratiometric images to remove any remaining background noises. As a result, a dark background is generated in each ratiometric image.

6. Use the **Freehand Selection** tool in FIJI-ImageJ to manually segment and calculate pixel intensities displayed on single cells. The pixel intensities correspond to the concentrations of the chemical bond that is being visualized.

7. Analyze the pixel intensities for statistical significance on an appropriate statistical software application. Here, GraphPad Prism was used. Repeat this analysis with the remaining ratiometric analysis.

## Representative Results

The addition of excess AAAs at 15x concentrations to the 50% $D_2O$-containing cell culture media produced distinct C-D Raman bands of newly synthesized lipids and proteins in

HeLa cells (Figure 2B). Previous experiments were performed with different concentration levels, such as 2x and 5x, and although the data is not presented, the 15x concentration produced the most distinct C-D Raman bands of newly synthesized lipids and proteins. Specifically, by investigating lipid droplets (LDs), we noticed that both 15x Phe and 15x Tryp induced newly synthesized lipids and protein signals at 2,143 $cm^{-1}$ and 2,172 $cm^{-1}$, respectively. DO-SRS was subsequently used to visualize the spatial distribution of C-D signals on single cells (Figure 3). Using ImageJ, pixel intensities of individual cells were manually segmented and calculated, as indicated by dotted-white borders in Figure 3A. The control cells display moderate C-D lipid and protein bands; however, the 15x Phe and 15x Tryp display stronger C-D lipid and protein bands. Quantitative analysis indicates that excess AAAs may upregulate lipid synthesis by 10%-17% but downregulate protein synthesis by 10% (Figure 3C,D). The results infer the possibility of a lack of autophagy that accumulates newly synthesized lipids, promotes mitochondrial dysfunction, and induces oxidative imbalance under excess AAA regulation[7].

Label-free multimodal SRS and 2PEF imaging of unsaturated lipid (~3,011 $cm^{-1}$), saturated lipid (~2,880 $cm^{-1}$), and NADH, Flavin were acquired to understand the effects of AAAs on cancer metabolism. Similarly, pixel intensities of individual cells were manually segmented and calculated using ImageJ, as indicated by dotted-white borders in Figure 3B. Ratiometric analysis of AAA-treated cells displays a 10% increase in unsaturated lipid/saturated lipid and a 50% increase in Flavin/Flavin + NADH (Figure 3E,F). In the electron transport chain of mitochondria, ROS can be generated from the transfer of electrons from NADH and $FADH_2$ to molecular oxygen species. The accumulation of ROS in many cancer cells results in an oxidative imbalance that oxidizes unsaturated fatty acids, promotes saturated fatty acid synthesis, and depletes NADH autofluorescence signals. Therefore, the observed increase in Flavin/Flavin + NADH is an indicator of accumulated ROS that reduces NADH autofluorescence signals. In response to oxidative imbalance, HeLa cells may upregulate their unsaturated lipid synthesis to replace the oxidized ones. This response is not observed in other cancer cell lines[29] , which signifies the metabolic heterogeneity of cancer cells under an excess AAA diet[30] .

In addition to multimodal imaging, SRS can reconstruct label-free 3D images of LDs in control and AAA-treated HeLa cells. In brief, microscopy generates a set of cross-sectional images throughout a selected region of interest. In this study, the stimulated Raman loss (SRL) was tuned to 2,845 $cm^{-1}$ and scanned from the top layer to the bottom layer with a step size of 1 μm (Figure 4A). Quantitative analyses of 3D lipid droplets reveal that LDs reduced in size but increased in counts in AAA-treated cells compared to the control (Figure 4B,C). The increased presence of bulky hydrophobic amino acids, such as Tryp and Phe may impair the function of LD-coating proteins. This ultimately reduces lipolysis, which accumulates numerous small LDs. The label-free 3D SRS volumetric imaging results of this study corroborate with previous studies by visualizing that excess AAA-treated cells exhibit numerous smaller LDs[31 , 32] .

## Discussion

DO-SRS and 2PEF imaging have been applied to investigate metabolic dynamics in various *ex vivo* models, including Drosophila and human tissues[21 , 22 , 23 , 24 , 26 , 27 , 33] . The imaging modality used in this study integrates DO-SRS and 2PEF microscopy, which can outpace other molecule-specific imaging methods by eliminating the need for molecule extraction or labeling with cytotoxic reagents and requiring minimal sample preparation. Specifically, DO-SRS microscopy enables us to probe *de novo* lipogenesis and protein synthesis in animals and cells and visualize their metabolic dynamics *in situ*[23 , 27 , 34] . 2PEF captures the autofluorescence signals of naturally occurring biomolecules, such as Flavin and NADH, in biological samples[35 , 36] . The imaging penetration depth of SRS can achieve up to 200-500 μm in less scattering samples[37] . With tissue-clearing methods such as urea, the penetration depth can increase more than tenfold[37] . The coupling of SRS with 2PEF enables us to image endogenous fluorophores such as Flavin and NADH in biological samples, which further eliminates the need for exogenous biomarkers for detection. 2PEF can achieve a penetration depth of 500 μm[38] . Compared to other multiplex imaging modalities, such as multi-color single-photon confocal fluorescence microscopy, both DO-SRS and 2PEF can achieve a significantly larger penetration depth without cytotoxic exogenous biomarkers.

To increase the spatial resolution of DO-SRS and 2PEF, we developed an adaptive moment estimation (Adam)-based pointillism deconvolution (A-PoD) image post-processing tool[34] . A-PoD can convert diffraction-limited DO-SRS and 2PEF images to super-resolved ones without the need for any hardware improvements. Additionally, the Raman spectrum contains many specific chemical vibration modes that can be harnessed to increase the number of detectable molecules. Taking this advantage, our lab has further generated a penalized reference matching (PRF) method to distinguish multiple lipid species in cell and tissue models[36] . These two technical developments open new avenues for studying biological processes in more detail at cellular and sub-cellular levels, which have been used to characterize metabolic changes in brain, cancer, and aging processes[26 , 27 , 35] .

One main limitation of this protocol is the concentration and time incubation of cellular samples with $D_2O$ to produce distinct, quantifiable C-D Raman bands. More robust, metabolically active cell lines, such as HeLa cells, can incorporate deuterium atoms into newly synthesized macromolecules at a faster rate than non-diseased mammalian cell lines, such as human embryonic kidney (HEK) cells, leading to various C-D intensities observed for the same concentration and time incubation with $D_2O$ in two different cell lines[21] . Furthermore, the administration of $D_2O$ at a concentration of 80% or above for 48 h may introduce toxicity to cellular samples. An optimization experiment to identify the optimal $D_2O$ concentration and time incubation is necessary to achieve desirable results.

A critical aspect of the protocol is the integration of DO-SRS and 2PEF imaging. Typically, DO-SRS and 2PEF modalities share the same picosecond excitation laser, as its narrow bandwidth can be optimized with SRS and 2PEF signals. Although our technology is homebuilt, this platform is commercially available[39] . Additional equipment, such as two synchronized laser pulses with a modulator, photodiode detector, a lock-in amplifier, and

a scanning microscope's joint efforts are required to detect the Raman signal. $D_2O$ can be readily purchased from biotechnology vendors. Therefore, researchers can access this technology very easily.

## Acknowledgments

We thank Dr. Yajuan Li and Anthony Fung for their technical support, and the Fraley lab for the cell line. We acknowledge the start-up funds from UCSD, NIH U54CA132378, NIH 5R01NS111039, NIH R21NS125395, NIHU54DK134301, NIHU54 HL165443, and Hellman Fellow Award.

## References

1. Wu G. Functional amino acids in nutrition and health. Amino Acids. 45 (3), 407–411 (2013). [PubMed: 23595206]
2. Wei Z, Liu X, Cheng C, Yu W, Yi P Metabolism of amino acids in cancer. Frontiers in Cell and Developmental Biology. 8, 603837 (2020). [PubMed: 33511116]
3. Parthasarathy A. et al. A three-ring circus: Metabolism of the three proteogenic aromatic amino acids and their role in the health of plants and animals. Frontiers in Molecular Biosciences. 5, 29 (2018). [PubMed: 29682508]
4. Wang H. et al. l-tryptophan activates mammalian target of rapamycin and enhances expression of tight junction proteins in intestinal porcine epithelial cells. The Journal of Nutrition. 145 (6), 1156–1162 (2015). [PubMed: 25878205]
5. Saxton RA, Sabatini DM mTOR signaling in growth, metabolism, and disease. Cell. 168 (6), 960–976 (2017). [PubMed: 28283069]
6. Mossmann D, Park S, Hall MN mTOR signalling and cellular metabolism are mutual determinants in cancer. Nature Reviews. Cancer 18 (12), 744–757 (2018). [PubMed: 30425336]
7. Kimura T, Watanabe Y Tryptophan protects hepatocytes against reactive oxygen species-dependent cell death via multiple pathways including Nrf2-dependent gene induction. Amino Acids. 48 (5), 1263–1274 (2016). [PubMed: 26795536]
8. Ma Q. et al. Dietary supplementation with aromatic amino acids decreased triglycerides and alleviated hepatic steatosis by stimulating bile acid synthesis in mice. Food and Function. 12 (1), 267–277 (2021). [PubMed: 33300530]
9. Cheng C. et al. Treatment implications of natural compounds targeting lipid metabolism in nonalcoholic fatty liver disease, obesity and cancer. International Journal of Biological Sciences. 15 (8), 1654–1663 (2019). [PubMed: 31360108]
10. Lubes G, Goodarzi M GC-MS based metabolomics used for the identification of cancer volatile organic compounds as biomarkers. Journal of Pharmaceutical and Biomedical Analysis. 147, 313–322 (2018). [PubMed: 28750734]
11. Di Gialleonardo V, Wilson DM, Keshari KR The potential of metabolic imaging. Seminars in Nuclear Medicine. 46 (1), 28–39 (2016). [PubMed: 26687855]
12. Bowman AP et al. Evaluation of lipid coverage and high spatial resolution MALDI-imaging capabilities of oversampling combined with laser post-ionisation. Analytical and Bioanalytical Chemistry. 412 (10), 2277–2289 (2020). [PubMed: 31879798]
13. Murphy RC, Hankin JA, Barkley RM Imaging of lipid species by MALDI mass spectrometry. Journal of Lipid Research. 50 Suppl, S317–S322 (2009). [PubMed: 19050313]
14. Pirman DA et al. Changes in cancer cell metabolism revealed by direct sample analysis with MALDI mass spectrometry. PLoS One. 8 (4), e61379 (2013). [PubMed: 23658609]
15. Li Z. et al. Single-cell lipidomics with high structural specificity by mass spectrometry. Nature Communications. 12 (1), 2869 (2021).
16. Miyagi M, Kasumov T Monitoring the synthesis of biomolecules using mass spectrometry. Philosophical Transactions. Series A, Mathematical, Physical and Engineering Sciences. 374 (2079), 20150378 (2016). [PubMed: 27644976]

17. Wang T, Shogomori H, Hara M, Yamada T, Kobayashi T Nanomechanical recognition of sphingomyelin-rich membrane domains by atomic force microscopy. Biochemistry. 51 (1), 74–82 (2012). [PubMed: 22148674]
18. Fung AA, Shi L Mammalian cell and tissue imaging using Raman and coherent Raman microscopy. Wiley Interdisciplinary Reviews. Systems Biology and Medicine. 12 (6), e1501 (2020). [PubMed: 32686297]
19. Shi L, Fung AA, Zhou A Advances in stimulated Raman scattering imaging for tissues and animals. Quantitative Imaging in Medicine and Surgery. 11 (3), 1078–1101 (2021). [PubMed: 33654679]
20. Yamakoshi H. et al. Imaging of EdU, an alkyne-tagged cell proliferation probe, by Raman microscopy. Journal of the American Chemical Society. 133 (16), 6102–6105 (2011). [PubMed: 21443184]
21. Shi L. et al. Optical imaging of metabolic dynamics in animals. Nature Communications. 9 (1), 2995 (2018).
22. Bagheri P, Hoang K, Fung AA, Hussain S, Shi L Visualizing cancer cell metabolic dynamics regulated with aromatic amino acids using DO-SRS and 2PEF microscopy. Frontiers in Molecular Biosciences. 8, 779702 (2021). [PubMed: 34977157]
23. Li Y. et al. Direct imaging of lipid metabolic changes in drosophila ovary during aging using DO-SRS microscopy. Frontiers in Aging. 2, 819903 (2022). [PubMed: 35822015]
24. Li Y, Zhang W, Fung AA, Shi L DO-SRS imaging of metabolic dynamics in aging Drosophila. Analyst. 146 (24), 7510–7519 (2021). [PubMed: 34781326]
25. Zhang L. et al. Spectral tracing of deuterium for imaging glucose metabolism. Nature Biomedical Engineering. 3 (5), 402–413 (2019).
26. Fung AA et al. Imaging sub-cellular methionine and insulin interplay in triple negative breast cancer lipid droplet metabolism. Frontiers in Oncology. 12, 858017 (2022). [PubMed: 35359364]
27. Li Y, Zhang W, Fung AA, Shi L DO-SRS imaging of diet regulated metabolic activities in Drosophila during aging processes. Aging Cell. 21 (4), e13586 (2022). [PubMed: 35257470]
28. Shi L, Wei M, Min W Highly-multiplexed tissue imaging with raman dyes. Journal of Visualized Experiments. (182), e63547 (2022).
29. Rysman E et al. De novo lipogenesis protects cancer cells from free radicals and chemotherapeutics by promoting membrane lipid saturation. Cancer Research. 70 (20), 8117–8126 (2010). [PubMed: 20876798]
30. Lisec J, Jaeger C, Rashid R, Munir R, Zaidi N Cancer cell lipid class homeostasis is altered under nutrient-deprivation but stable under hypoxia. BMC Cancer. 19 (1), 501 (2019). [PubMed: 31138183]
31. Thiam AR, Dugail I Lipid droplet-membrane contact sites - from protein binding to function. Journal of Cell Science. 132 (12), jcs230169 (2019). [PubMed: 31209063]
32. Schott MB et al. Lipid droplet size directs lipolysis and lipophagy catabolism in hepatocytes. The Journal of Cell Biology. 218 (10), 3320–3335 (2019). [PubMed: 31391210]
33. Hoang K. et al. Subcellular resolution DO-SRS and 2PEF imaging of metabolic dynamics regulated by L-methionine in amyotrophic lateral sclerosis. In Optical Biopsy XXI: Toward Real-Time Spectroscopic Imaging and Diagnosis. SPIE. 1237303, 6–13 (2023).
34. Jang H. et al. Super-resolution stimulated Raman scattering microscopy with A-PoD. bioRxiv. 10.1101/2022.06.04.4948132022.2006.2004.494813 (2022).
35. Li Y. et al. Optical metabolic imaging uncovers sex- and diet-dependent lipid changes in aging drosophila brain. bioRxiv. 10.1101/2022.10.01.5104162022.2010.2001.510416 (2022).
36. Zhang W. et al. Multi-molecular hyperspectral PRM-SRS imaging. bioRxiv. 10.1101/2022.07.25.5014722022.2007.2025.501472 (2022).
37. Wei M. et al. Volumetric chemical imaging by clearing-enhanced stimulated Raman scattering microscopy. Proceedings of the National Academy of Sciences. 116 (14), 6608–6617 (2019).
38. Chang T. et al. Non-invasive monitoring of cell metabolism and lipid production in 3D engineered human adipose tissues using label-free multiphoton microscopy. Biomaterials. 34 (34), 8607–8616 (2013). [PubMed: 23932290]

39. Leica Microsystems. Leica TCS SP8 CARS CARS Microscope - Label Free Imaging., <https://www.leica-microsystems.com/products/confocal-microscopes/p/leica-tcs-sp8-cars/downloads/> (2023).

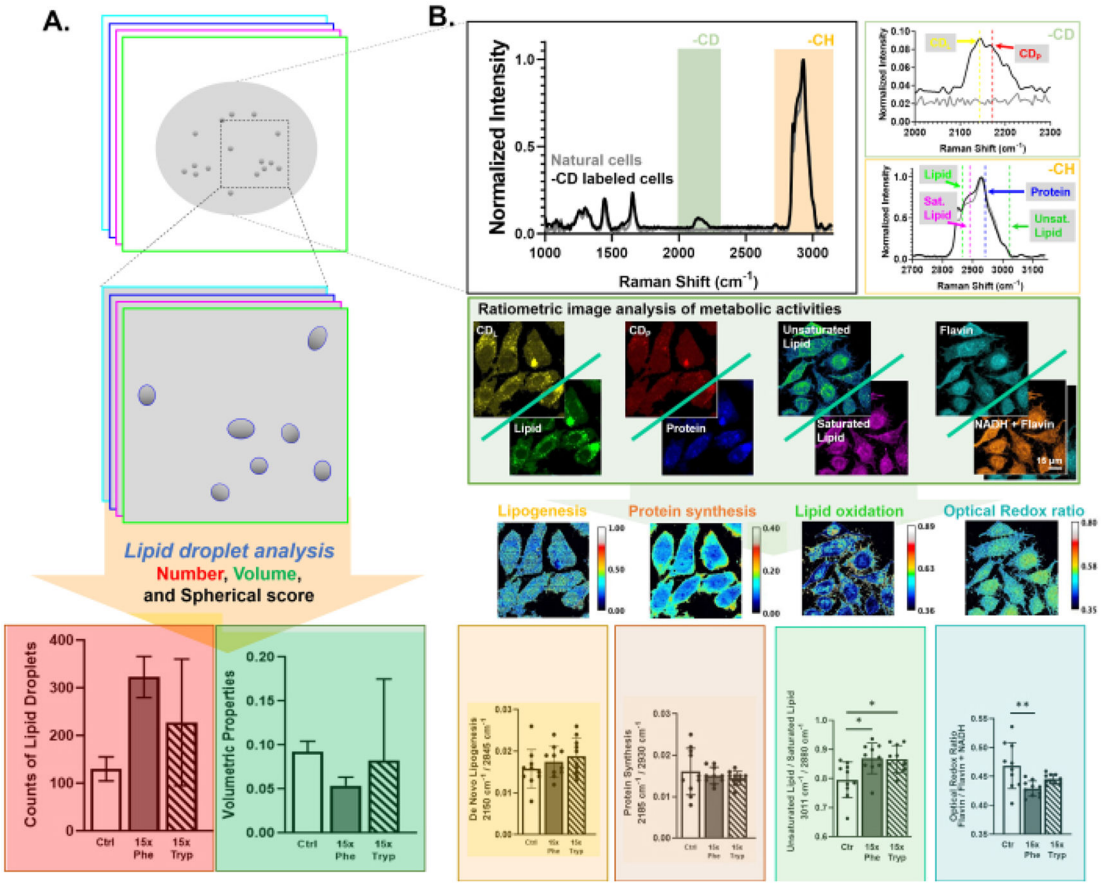


**Figure 1: An illustration of the image acquisition and analysis with DO-SRS and 2PEF.**

(**A**) A 3D image reconstruction and analysis to acquire lipid droplet number, volume, and spherical score. (**B**) Hyperspectral imaging and analysis of deuterium-labeled lipid ($CD_L$; 2,145 $cm^{-1}$), lipid (2,845 $cm^{-1}$), deuterium-labeled protein ($CD_P$; 2,175 $cm^{-1}$), protein (2,940 $cm^{-1}$), unsaturated lipid (3,011 $cm^{-1}$), saturated lipid (2,880 $cm^{-1}$), NADH, and Flavin.

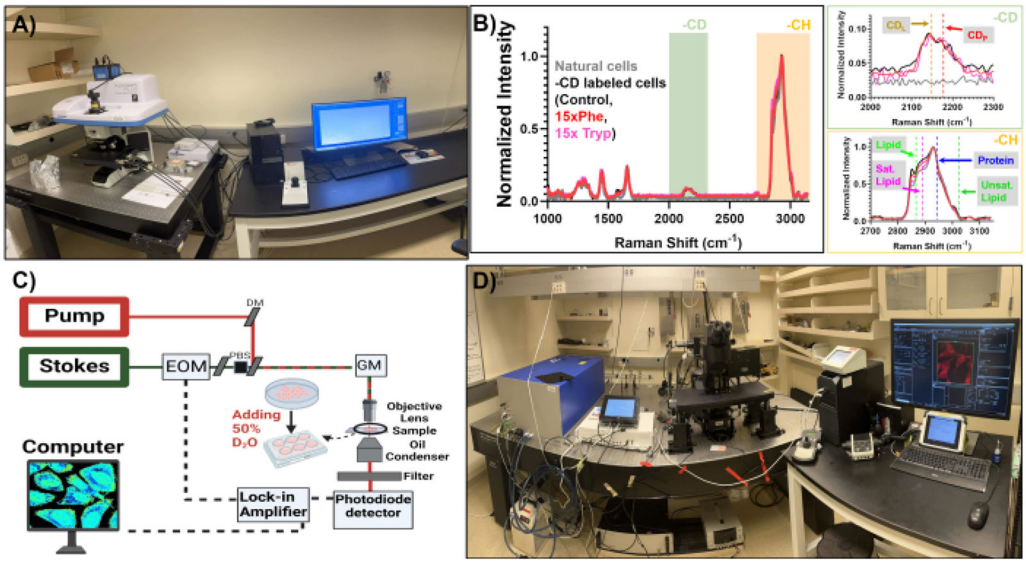


**Figure 2: Physical setup of spontaneous Raman spectroscopy and stimulated Raman scattering microscopy.**

(**A**) Spontaneous Raman spectroscopy setup used for this study. (**B**) Sample spontaneous Raman spectra for CD label (red), without CD label (black), control group (blue, solid line), 15x Phe-treated group (red, dotted line), and 15x Tryp-treated group (pink, dotted line). (**C**) Schematic diagram of the stimulated Raman scattering microscopy setup used for this investigation. (**D**) Stimulated Raman scattering microscopy setup used as the DO-SRS and 2PEF platform.

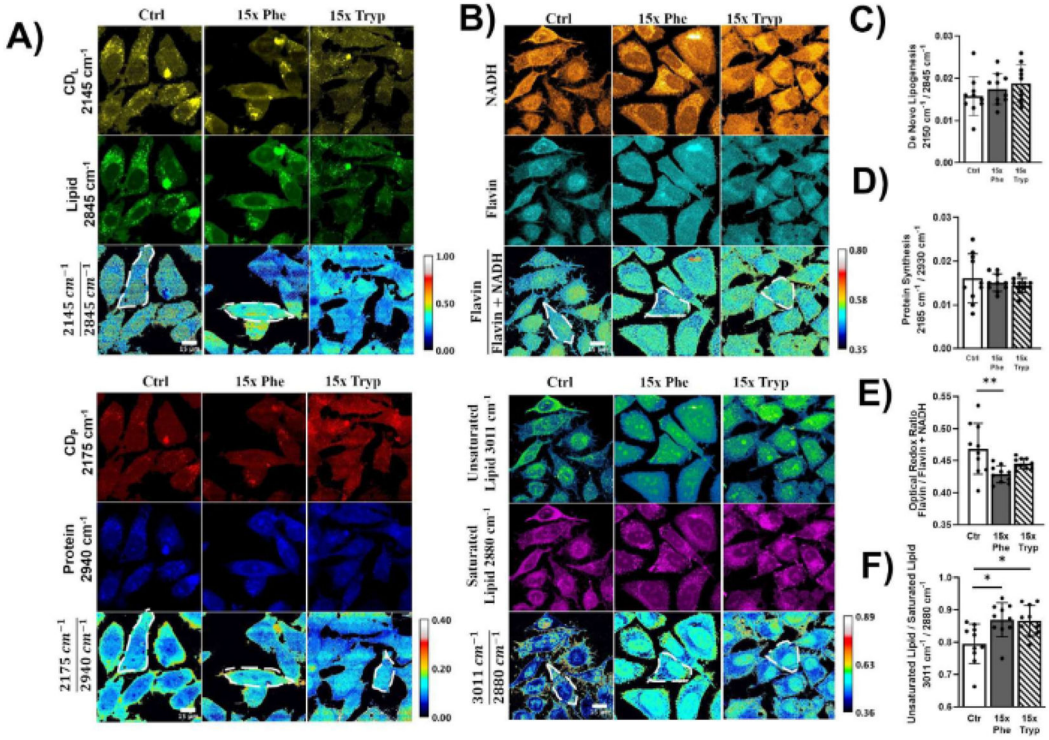


**Figure 3: Visualizing metabolic dynamics in HeLa cells using DO-SRS and 2PEF microscopy.**

(**A**) Deuterium-labeled lipid (2,145 $cm^{-1}$), lipid (2,845 $cm^{-1}$), deuterium-labeled protein (2,175 $cm^{-1}$), protein (2,940 $cm^{-1}$) visualized in HeLa cells under control (Ctrl), 15x phenylalanine (15x Phe), and 15x tryptophan (15x Tryp) with the DO-SRS platform. Lipid turnover rate and protein turnover rate were calculated as $\frac{2145\,cm^{-1}}{2845\,cm^{-1}}$ and $\frac{2175\,cm^{-1}}{2940\,cm^{-1}}$. Raw images were first subtracted by the PBS signal to remove background intensity and masked to remove intensity outside of the cells using ImageJ. Pixel-wise division was performed for the ratiometric analysis. (**B**) NADH and Flavin channels visualized with 2PEF microscopy, and unsaturated lipid (3,011 $cm^{-1}$) and saturated lipid (2,880 $cm^{-1}$) visualized with label-free SRS microscopy. Optical redox ratio and saturation ratio were calculated with $\frac{Flavin}{Flavin+NADH}$ and $\frac{3011\,cm^{-1}}{2880\,cm^{-1}}$. (**C-F**) Quantification of ratiometric intensities for each HeLa cell under control, 15x Phe, and 15x Tryp conditions. The statistical difference was used to compare excess AAA conditions with the control conditions. ****$p < 0.0001$, ***$p < 0.001$, **$p < 0.01$, *$p < 0.05$ were calculated from a two-way ANOVA test.

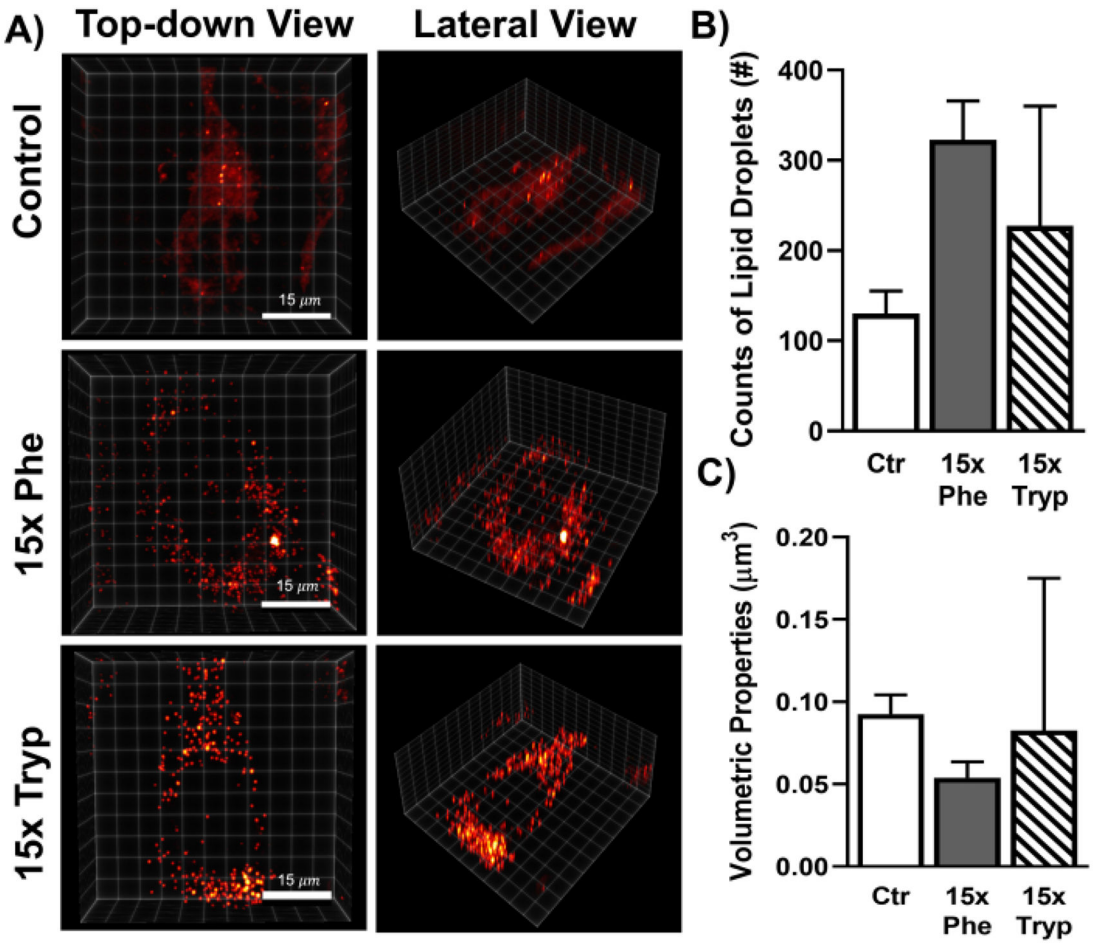


**Figure 4: Visualization of 3D lipid droplet distribution of a single HeLa cell using a label-free SRS microscope.**

(**A**) SRS 3D lipid droplet volume projection in HeLa cells under control and excess AAA conditions. The threshold was defined prior to the analysis, revealing lipid droplet signal distribution. (**B,C**) Quantification of lipid droplet volume and counts within individual HeLa cells under control group and excess AAA conditions using the two-way ANOVA test.